Taylor & Francis
Taylor & Francis Group

RESEARCH ARTICLE

🔓 OPEN ACCESS | Check for updates

Electrophysiological characterization of sourced human iPSC-derived motor neurons

Bohumila Jurkovicova-Tarabova [a,b], Robin N. Stringer [c], Zuzana Sevcikova Tomaskova [a], and Norbert Weiss [c,a]

aInstitute of Molecular Physiology and Genetics, Center of Biosciences, Slovak Academy of Sciences, Bratislava, Slovakia; bDepartment of Biology, Faculty of Education, Trnava University, Trnava, Slovakia; cDepartment of Pathophysiology, Third Faculty of Medicine, Charles University, Prague, Czech Republic

ABSTRACT

Induced pluripotent stem cell (iPSC)-derived motor neurons provide a powerful platform for studying motor neuron diseases. These cells enable human-specific modeling of disease mechanisms and high-throughput drug screening. While commercially available iPSC-derived motor neurons offer a convenient alternative to time-intensive differentiation protocols, their electrophysiological properties and maturation require comprehensive evaluation to validate their utility for research and therapeutic applications. In this study, we characterized the electrophysiological properties of commercially available iPSC-derived motor neurons. Immunofluorescence confirmed the expression of motor neuron-specific biomarkers, indicating successful differentiation and maturation. Electrophysiological recordings revealed stable passive membrane properties, maturation-dependent improvements in action potential kinetics, and progressive increases in repetitive firing. Voltage-clamp analyses confirmed the functional expression of key ion channels, including high- and low-voltage-activated calcium channels, TTX-sensitive and TTX-insensitive sodium channels, and voltage-gated potassium channels. While the neurons exhibited hallmark features of motor neuron physiology, high input resistance, depolarized resting membrane potentials, and limited firing capacity suggest incomplete electrical maturation. Altogether, these findings underscore the potential of commercially available iPSC-derived motor neurons as a practical resource for MND research, while highlighting the need for optimized protocols to support prolonged culture and full maturation.

Introduction

Induced pluripotent stem cells (iPSCs) have revolutionized biomedical research, providing a versatile platform for modeling human diseases, particularly neurological disorders. iPSC-derived motor neurons are of particular interest for studying the pathophysiology of motor neuron diseases (MNDs) such as amyotrophic lateral sclerosis (ALS) and spinal muscular atrophy (SMA) [1–3]. These cells offer a unique opportunity to investigate human-specific cellular and molecular mechanisms, providing insights that may be unattainable through animal models due to species-specific differences. Furthermore, iPSC-derived motor neurons serve as an invaluable tool for high-throughput drug screening, enabling the

identification of potential therapeutic candidates [4–7]. However, generating in-house human motor neurons is an arduous process requiring the reprogramming somatic cells, rigorous validation of pluripotency, and the optimization of differentiation protocols to reliably yield motor neuron populations. This is followed by an extended maturation period, all of which demand weeks to months of work, and highly specialized expertise to ensure reproducibility and reliability [8–10]. As an alternative, commercially available human iPSC-derived motor neurons have emerged as a practical and time-efficient option, providing ready-to-use, pre-differentiated motor neuron populations [11–13]. These pre-validated cells bypass the need for time-intensive differentiation

protocols, making them an appealing choice for disease modeling and drug discovery workflows.

MNDs are characterized by the progressive degeneration of motor neurons, often accompanied by alterations in their intrinsic excitability properties and ion channel function [14–16]. The dysfunction of ion channels, in particular, is thought to contribute to pathological changes in neuronal excitability and degeneration, underscoring the need for electrophysiological studies to understand these mechanisms. Therefore, the comprehensive characterization of the electrophysiological properties of iPSC-derived motor neurons in critical to validate their physiological relevance and to establish their suitability as models for MND research.

In this study, we aimed to characterize the electrophysiological properties of commercially available human iPSC-derived motor neurons. Using whole-cell patch clamp recordings, we assessed their passive membrane properties, action potential kinetics, and repetitive firing patterns, as well as the functional expression of voltage-gated calcium, sodium, and potassium channels. By providing a detailed electrophysiological profile of these cells, our study contributes to deeper understanding of their functional maturity and utility in MND modeling and therapeutic screening applications.

Materials and methods

Culture of iPSC-derived motor neurons

Human iPSC-derived motor neurons were obtained from Applied StemCell Inc., USA (ASE-9701, starter kit, African-American male line). The cells were cultured following the manufacturer's protocol. Briefly, frozen cells were thawed and plated onto coverslips pre-coated as per the protocol. They were grown in motor neuron basal culture medium supplemented with motor neuron culture media supplement A, both provided by the manufacturer. Cells were maintained at 37°C in a humidified atmosphere with 5% CO_2. To ensure optimal growth conditions, 50% of the culture medium was replaced every 2–3 days.

Immunostaining and confocal imaging

Differentiated motor neurons cultured on coverslips were fixed in ice-cold methanol immediately after electrophysiological recordings. Cells were immunostained at developmental stages DIV 2, DIV 10, and DIV 15 for late-stage motor neuron markers MNX1/HB9 (motor neuron and pancreas homeobox 1/homeobox HB9) and Tuj1 (class III β-tubulin) using rabbit monoclonal anti-MNX1/HB9 (Sigma #ABN174) and mouse monoclonal anti-Tuj1 (R&D Systems #MAB1195) antibodies, respectively. Cells were also stained at DIV 5, DIV 10, and DIV 14 for mature motor neuron markers CHAT (choline acetyltransferase) and MAP2 (microtubule-associated protein 2) using goat polyclonal anti-CHAT (R&D Systems #AF3447) and mouse monoclonal anti-MAP2 (Sigma #M4403) antibodies, respectively. Primary antibodies were prepared in 5% bovine serum albumin (BSA) with the following dilutions: HB9 (1:1000), Tuj1 (1:500), CHAT (1:300), and MAP2 (1:1000). Coverslips were incubated with the primary antibodies for 1 hour at room temperature (RT), washed with PBS containing 0.05% Tween 20, and incubated with the following secondary antibodies: anti-rabbit Alexa 594 (Invitrogen #A-21207) for MNX1/HB9, anti-mouse Alexa 488 (Invitrogen # A-11001) for TuJ1, anti-goat Alexa 488 (Abcam # ab150129) for CHAT, and anti-mouse Alexa 546 (Invitrogen # A-11003) for MAP2, at a 1:1000 dilution for 1 hour in the dark at RT. Coverslips were mounted using Fluoroshield (Sigma) and analyzed by fluorescence microscopy. Photomicrographs were captured with a Leica SP8 DMi8 fluorescence microscope equipped with a 63× oil-immersion objective. Fluorescence images were acquired using a Leica DFC340 FX digital camera and processed with Leica Advanced Fluorescence software. Image analysis (quantification and merging) was performed with the open-source software ImageJ. The fluorescence intensity of each cell was quantified as $I_{fluorescence}$ = integrated density – (area x mean background fluorescence).

Electrophysiological recordings

Electrophysiological recordings of action potentials (APs) were performed from day 5 in vitro (DIV 5) to DIV 15, while whole-cell current recordings were conducted at DIV 10. Recordings were carried out using a HEKA-10 amplifier controlled by

Patchmaster software v90.2 (HEKA Electronics, Germany). Patch pipettes with a resistance of 2.3–3.0 MΩ were used, and only cells with a series resistance below 5 MΩ were included in the analysis. Cell capacitance and series resistance were monitored after membrane rupture and compensated online by up to 70% using the built-in circuitry of the EPC-10 amplifier. Linear capacitance and leak currents were subtracted using the P/4 protocol. All recordings were performed at room temperature (22–25 °C).

For AP recordings, the extracellular solution contained (in mM): 125 NaCl, 3 KCl, 1.2 $CaCl_2$, 1 $MgSO_4$, 25 $NaHCO_3$, 1.25 NaH_2PO_4, 10 glucose, 3 myo-inositol, 3 Na-pyruvate, and 0.5 L-ascorbic acid, adjusted to pH 7.4 with 5% O_2/95% CO_2. The pipette solution contained (in mM): 120 K-gluconate, 20 KCl, 2 $MgCl_2$, 2 Na-ATP, 0.25 Na-GTP, and 10 hEPES, adjusted to pH 7.4 with KOH. Recordings were performed in current-clamp mode using the whole-cell configuration, with the holding current adjusted to maintain a resting membrane potential of approximately −70 mV. Single APs were elicited by 5-ms depolarizing current pulses ranging from −60 pA to +300 pA in 20-pA increments. For repetitive firing analysis, 500-ms depolarizing current pulses were applied. Input resistance was assessed using a series of six 250-ms hyperpolarizing current pulses, starting at 0 pA and decreasing in 25-pA increments.

For voltage-activated calcium current recordings, the extracellular solution contained (in mM): 140 TEA-Cl, 10 $CaCl_2$, and 10 hEPES, adjusted to pH 7.4 with CsOH. The pipette solution contained (in mM): 130 $CsCH_3SO_3$, 10 TEA-Cl, 5 $MgCl_2$, 10 EGTA, 5 Na-ATP, and 10 hEPES, adjusted to pH 7.4 with KOH. Recordings of high-voltage-activated (HVA) calcium currents were conducted from a holding potential of −80 mV, while low-voltage-activated (LVA) calcium currents were recorded from a holding potential of −100 mV. The current-voltage (I/V) relationship for HVA currents was assessed using 150-ms depolarizing pulses ranging from −70 mV to +60 mV in 10-mV increments. LVA currents were evaluated using similar pulses ranging from −100 to 0 mV. Specific blockers were used to identify individual HVA conductances: Nifedipine (10 μM) for L-type channels, ω-Conotoxin GVIA (2 μM) for N-type channels, ω-Agatoxin IVA (600 nM) for P/Q-type channels, and SNX-482 (200 nM) for R-type channels. Stock solutions of blockers were prepared and diluted to the final concentrations in the external solution immediately before experiments. The effects of calcium channel blockers were assessed by applying 150-ms depolarizing pulses to the voltage eliciting the maximal current amplitude.

For voltage-activated sodium current recordings, the extracellular solution contained (in mM): 105 NaCl, 2 $CaCl_2$, 0.5 $MgCl_2$, 10 hEPES, 25 TEA-Cl, and 10 glucose, adjusted to pH 7.4 with NaOH. The pipette solution contained (in mM): 135 CsCl, 10 EGTA, 1 $MgCl_2$, 3 NaCl, 0.5 $CaCl_2$, 4 Na-ATP, 0.3 Na-GTP, and 10 hEPES, adjusted to pH 7.4 with CsOH. Recordings were performed from a holding potential of −100 mV. The I/V relationship was determined using 20-ms depolarizing pulses ranging from −70 mV to +50 mV in 10-mV increments. To confirm the TTX sensitivity of sodium currents, recordings were repeated in the presence of 1 μM TTX. TTX was prepared as a 1 mm stock solution and diluted to the final concentration in the external solution before use.

For voltage-activated potassium current recordings, the extracellular solution contained (in mM): 130 NaCl, 3 KCl, 2 $CaCl_2$, 1 $MgCl_2$, 10 hEPES, and 10 glucose, adjusted to pH 7.4 with NaOH. The pipette solution contained (in mM): 120 K-gluconate, 20 KCl, 2 $MgCl_2$, 2 Na-ATP, 0.25 Na-GTP, and 10 hEPES, adjusted to pH 7.4 with KOH. Recordings were conducted from a holding potential of −60 mV. The I/V relationship were measured using 400-ms depolarizing pulses ranging from −40 mV to +80 mV in 10-mV increments.

Electrophysiological analysis

Analysis of action potential recordings (input resistance, single action potential properties, and repetitive firing) was performed offline using Easy Electrophysiology software (Easy Electrophysiology Software LtD, England). Analysis of ion current was performed offline by HEKA Fitmaster v2×91(HEKA Electronics,

Germany), OriginPro 2024b software (OriginLab Company, USA) and GraphPad Prism (GraphPad Software Inc., USA). The current-voltage relationship (I/V) curves were fitted with the following modified Boltzmann Equation (1):

$$I(V) = Gmax \frac{(V - Vrev)}{1 + exp \frac{(V0.5 - V)}{k}}$$

with $I(V)$ being the peak current amplitude at the command potential V, G_{max} the maximum conductance, V_{rev} the reversal potential, $V_{0.5}$ the half-activation potential, and k the slope factor.

The voltage-dependence of the whole-cell conductance was calculated using the following modified Boltzmann Equation (2):

$$G(V) = Gmax \frac{Gmax}{1 + exp \frac{(V0.5 - V)}{k}}$$

with $G(V)$ being the conductance at the command potential V.

In part of experiments with calcium current blockers, the raw recordings were corrected for run-down according to the following Equation (3):

$$Icorrected = Imeasured$$
$$+ \left(Imax - \left(y0 + A1 * exp \left(\frac{t}{\tau} \right) \right) \right)$$

with $I_{corrected}$ being the corrected current amplitude, $I_{measured}$ the current amplitude measured during the experiment, I_{max} the maximal current amplitude measured at the beginning of the recording, y_0 the steady-state current amplitude to which the current amplitude converged during run-down, A_1 the amplitude of the mono-exponential curve at $t = 0$, τ the time constant and t the time.

Statistics

Data values are presented as mean ± S.E.M for n measurements. Unpaired Student's t test (unless stated otherwise) was carried out to test for statistical significance and data sets were considered different for $p < 0.05$.

Results

Confirmation of motor neuron identity in iPSC-derived cultures

To confirm the motor neuron identity of the human iPSC-derived cells used for electrophysiological analyses, we performed immunofluorescence staining to assess the expression of motor neuron-specific markers at various developmental stages in vitro (DIV). The iPSC-derived motor neurons expressed late-stage precursor markers, including MNX1/HB9 and Tuj1, from DIV 2 to DIV 15 (Figure 1(a)). The expression of MNX1/HB9 significantly decreased from DIV 2 to DIV 10 and DIV 15 (Figure 1(b)) indicating differentiation toward a mature motor neuron phenotype, consistent with previous reports [17]. Additionally, these cells exhibited expression of mature motor neuron markers such as CHAT and MAP2 from DIV 5 to DIV 15 (Figure 1(c,d)), confirming the maturation of the motor neurons. The co-expression of these markers across multiple time points further supports the successful differentiation of the iPSCs into motor neurons. These results demonstrate that the iPSC-derived cells undergo appropriate differentiation into both precursor and mature motor neuron stages, providing a reliable model for subsequent electrophysiological investigations.

Passive membrane properties of iPSC-derived motor neurons

To evaluate the passive membrane properties of iPSC-derived motor neurons, we performed patch-clamp recordings across two time periods: 5–8 days (DIV 5–8) and 9–15 days (DIV 9–15) post-plating. The resting membrane potential (RMP) was consistent between the two groups ($p = 0.8796$) with an average of -34.9 ± 1.8 mV ($n = 35$) at DIV 5–8 and -34.5 ± 1.3 mV ($n = 35$) at DIV 9–15 (Figure 2(a)). The input resistance was evaluated by injecting small hyperpolarizing currents and fitting the resulting linear subthreshold I/V relationship (Figure 2(b)). The input resistance values were also comparable between the two groups ($p = 0.7637$), with an average of 772.8 ± 40.7 MΩ ($n = 35$) at DIV 5–8 and 754.0 ± 46.1 MΩ ($n = 35$) at DIV 9–15 (Figure 2(c)). These results indicate that the passive membrane properties of
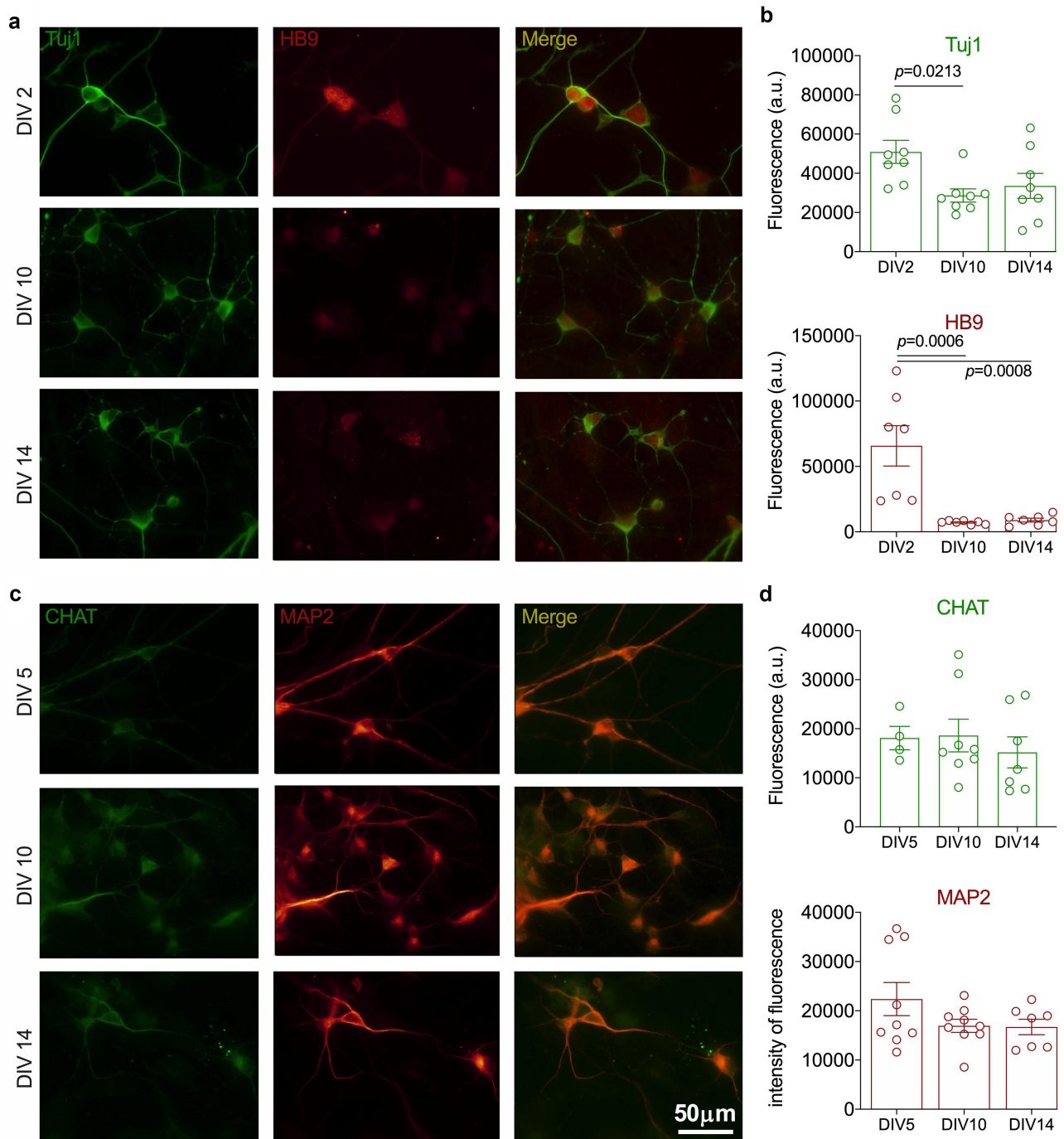
Figure 1. Immunostaining of iPSC-derived motor neurons for neuronal markers. (a) Confocal images of cryopreserved motor neurons stained for motor neuron late-stage precursor markers, Tuj1 (green) and MNX1/HB9 (red) at DIV 2 (top panels), DIV 10 (middle panels), and DIV 14 (bottom panels). (b) Corresponding fluorescence intensity quantification. (c) The cells were also stained for mature motor neuron markers, CHAT (green) and pan-neuronal maker MAP2 (red) at DIV 5 (top panels), DIV 10 (middle panels), and DIV 14 (bottom panels). (d) Corresponding fluorescence intensity quantification. Scale applies to both panels. Statistical analysis was conducted using ANOVA followed by Tukey's multiple comparison test.

the iPSC-derived motor neurons remain stable throughout the observed culture period. It is worth noting that recordings were performed daily from DIV 5 to DIV 15 and day-to-day comparisons with each group (DIV 5–8 and DIV 9–15) revealed no significant differences (ANOVA, data not shown). Altogether, the consistency in resting membrane potential and input resistance suggests that these properties are largely maintained as the neurons develop within this timeframe.
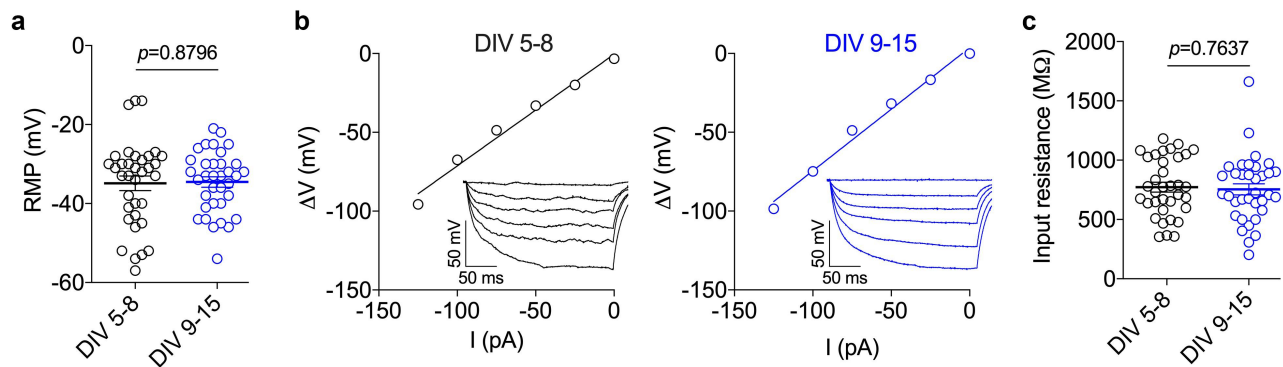
Figure 2. Passive membrane properties of iPSC-derived motor neurons. (a) Resting membrane potential values at two developmental stages: DIV 5–8 (black circles) and DIV 9–15 (blue circles). (b) Representative voltage traces in response to hyperpolarizing current injections and corresponding *I/V* relationship used to assess the input resistance. (c) Corresponding input resistance values of iPSC-derived motor neurons.

Single action potential properties of iPSC-derived motor neurons

We next investigated the action potential properties of iPSC-derived motor neurons. Single action potentials were evoked using brief 5-ms depolarizing current injections of 280 pA, as this condition produced the highest proportion of neurons with well-isolated, fully developed action potentials (Figure 3(a)). A significant difference ($p < 0.0001$) of the action potential threshold was observed between the two groups. Neurons at DIV 5–8 exhibited an action
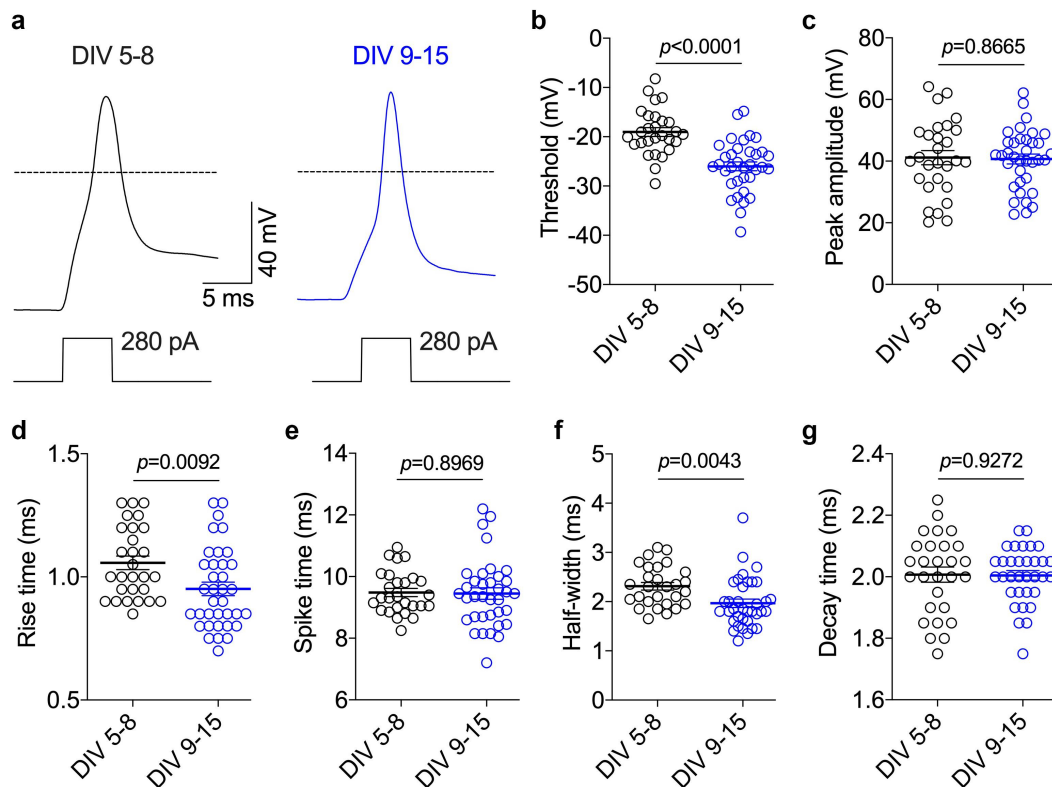

Figure 3. Single action potential analysis of iPSC-derived motor neurons. (a) Representative voltage traces of single action potentials recorded at two developmental stages: DIV 5–8 (black circles) and DIV 9–15 (blue circles). Actions potentials were elicited by 5-ms depolarizing current pulses of 280 pA, applied from a holding current adjusted to maintain a resting membrane potential of approximately −70 mV. Corresponding (b) Threshold potential values, (c) Peak amplitude values, (d) Rise time values, (e) Spike time values, (f) Half-width values, and (g) Decay time values.

potential threshold of -19.0 ± 0.9 mV ($n = 28$), whereas neurons at DIV 9–15 displayed a significantly lower threshold at -27.0 ± 1.3 mV ($n = 35$) (Figure 3(b)). We also observed small but significant differences in the rise time and half-width of action potentials between the two groups. Neurons at DIV 9–15 exhibited a faster ($p = 0.0092$) rise time (0.95 ± 0.03 ms, $n = 35$) compared to DIV 5–8 neurons (1.06 ± 0.03 ms, $n = 28$) (Figure 3(d)). Similarly, the half-width of action potentials was shorter ($p = 0.0043$) in DIV 9–15 neurons (1.97 ± 0.08 ms, $n = 35$) compared to DIV 5–8 neurons (2.31 ± 0.08 ms, $n = 28$) (Figure 3(f)). In contrast, no significant differences were detected in the peak amplitude (41.1 ± 2.3 mV at DIV 5–8 versus 40.7 ± 1.6 mV at DIV 9–15, Figure 3(c)), spike time (9.5 ± 0.1 ms at DIV 5–8 versus 9.5 ± 0.2 ms at DIV 9–15, Figure 3(e)), and decay time (2.00 ± 0.02 ms at DIV 5–8 versus 2.00 ± 0.02 ms at DIV 9–15, Figure 3(g)). These findings suggest that while neurons undergo modest maturation-related changes in certain parameters, such as threshold, rise time, and half-width, other properties, including action potential amplitude and decay dynamics, remain stable during the examined culture period. Collectively, these results indicate that iPSC-derived motor neurons exhibit limited maturation in action potential kinetics from 5 to 15 days post-plating.

Repetitive firing properties of iPSC-derived motor neurons

We next investigated the excitability of iPSC-derived motor neurons in response to sustained membrane depolarization. Action potentials were evoked using 500-ms depolarizing current injections of 20 pA, as this condition produced the highest number of action potentials during the depolarizing step. Only fully fledged action potentials that exceeded a rise rate above 15 mV/ms (assessed from phase plots) were included in our analysis. Our results revealed a significant trend toward increased neuronal firing from DIV 5–8 to DIV 9–15 (Chi-square test, $p < 0.0001$). Indeed, the neurons displayed four distinct firing patterns: non-firing neurons, which accounted for 59% of

cells at DIV 5–8 and 22% at DIV 9–15; neurons eliciting a single action potential, representing 30% of cells at DIV 5–8 and 48% at DIV 9–15; neurons generating 2–3 action potentials, which comprised 8% of cells at DIV 5–8 and 22% at DIV 9–15; and neurons firing 4–9 action potentials, which accounted for 3% of cells at DIV 5–8 and 8% at DIV 9–15 (Figure 4(a–c)). The shift in firing patterns over time suggests a maturation of electrophysiological properties as the neurons develop in culture. However, due to the low proportion of neurons firing 4–9 action potentials, we were unable to reliably extract additional metrics such as interspike intervals or perform more detailed analyses of action potential properties within this subset. Overall, these results highlight both the developmental progression and variability in the repetitive firing behavior of iPSC-derived motor neurons during the assessed culture period.

Voltage-gated ion channels in iPSC-derived motor neurons

To further characterize the electrophysiological properties of iPSC-derived motor neurons, we conducted voltage-clamp recordings to assess the presence and functionality of voltage-gated calcium, sodium, and potassium channels. Recordings were performed at DIV 10, at a time point were the cells exhibited the highest level of electrophysiological maturation and optimal health. Whole-cell patch clamp recordings revealed robust high-voltage-activated (HVA) calcium currents (Figure 5(a,b)) and comparatively smaller low-voltage-activated (LVA) T-type calcium currents (Figure 5(c,d)). The maximal macroscopic conductance for HVA calcium currents was 0.59 ± 0.06 nS/pF ($n = 30$), compared to 0.03 ± 0.01 nS/pF ($n = 10$) for LVA calcium currents (Figure 5(e)). The mean half-activation potential of HVA currents was $+7.8 \pm 1.2$ mV ($n = 30$), while LVA calcium currents exhibited a more hyperpolarized voltage dependence with a half-activation potential of -28.6 ± 1.3 mV ($n = 10$) (Figure 5(f,g)). These findings are consistent with the expected voltage dependence of HVA and LVA channels, respectively. To further dissect the contributions of various HVA channel subtypes to the total HVA current, we conducted a pharmacological analysis using selective blockers for specific HVA
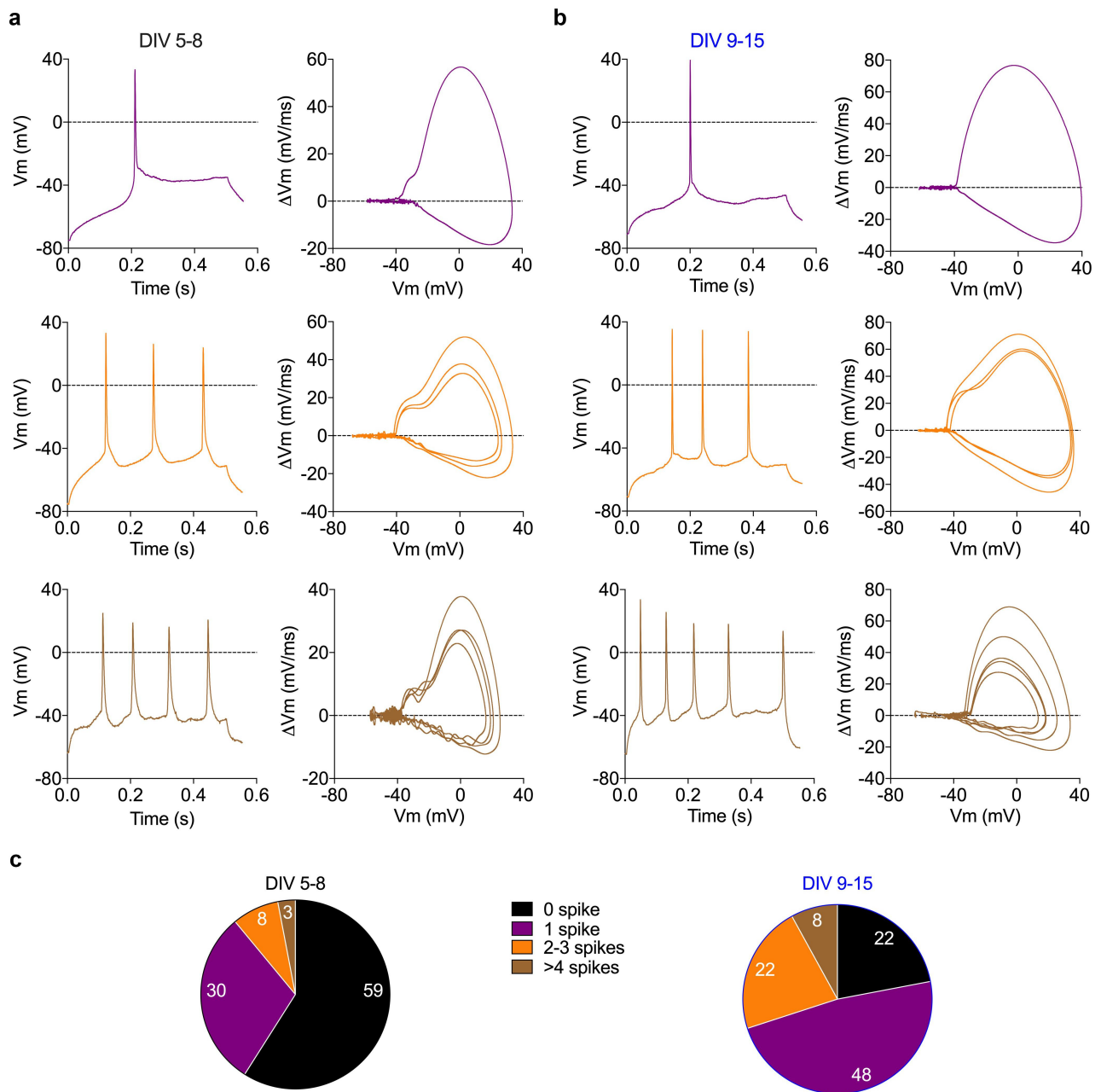
Figure 4. Repetitive firing analysis of iPSC-derived motor neurons. A Representative voltage traces recorded from iPSC-derived motor neurons at development stage DIV 5–8 (left panels), elicited by 500-ms depolarizing current pulses of 20 pA. The holding current adjusted to maintain a resting membrane potential was approximately −70 mV. The traces demonstrate different firing patterns: 1 AP (purple), 2–3 APs (orange), and > 4 APs (brown). Corresponding phase plots are shown in the right panels. B same as (A), but for iPSC-derived motor neurons at development stage DIV 9–15. C corresponding percentage of cells exhibiting different firing patterns: no response (black), 1 AP (purple), 2–3 APs (orange), and > 4 APs (brown).

calcium channels. Application of nifedipine (L-type current), ω-Conotoxin GVIA (N-type current), ω-Agatoxin IVA (P/Q-type current), and SNX-482 (R-type current) reduced the total HVA calcium current by 36%, 29%, 15%, and 20% respectively (Figure 5(h,i)). Next, we assessed voltage-gated sodium currents. We observed robust voltage-activated sodium currents that were partially blocked by 1 mm TTX (Figure 6(a,b)). For instance, TTX reduced the maximal conductance by 65% (paired Student's t test, $p < 0.0001$) from 0.60 ± 0.06 nS/pF to 0.21 ± 0.03 nS/pF ($n = 15$) (Figure 6(c)). The partial block observed with TTX suggests that iPSC-derived motor neurons express both TTX-sensitive and
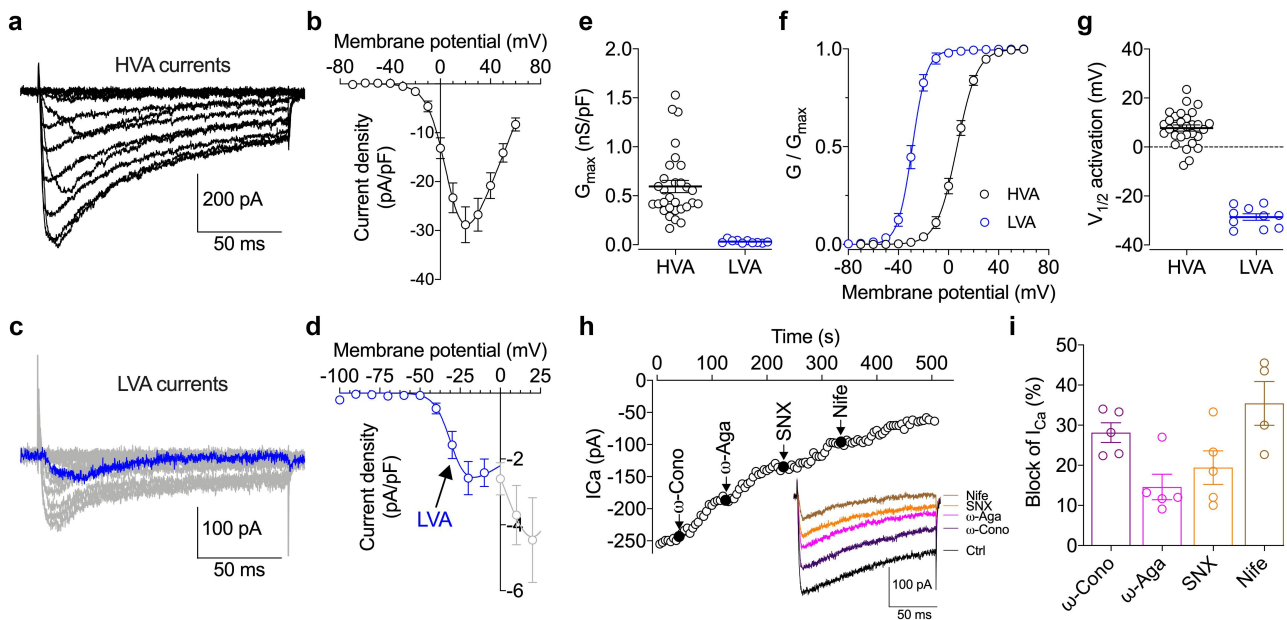
Figure 5. Voltage-activated calcium current analysis of iPSC-derived motor neurons. A Representative high-voltage activated (HVA) calcium current traces recorded from iPSC-derived motor neurons at DIV 10. Currents were elicited by 150-ms depolarizing steps ranging from −70 mV to +60 mV, applied from a holding potential of −80 mV. B corresponding mean I/V relationship for HVA calcium currents. C Representative voltage-activated calcium current traces recorded in the presence of a cocktail of HVA channel blockers (2 µM ω-conotoxin GVIA, 600 nM ω-agatoxin IVA, 200 nM SNX-482, and 10 µM nifedipine) to isolate low-voltage-activated (LVA, T-type) calcium currents. Currents were recorded from a holding membrane potential of −100 mV. A representative LVA current trace recorded at −30 mV is shown in blue. D corresponding mean I/V relationship for LVA currents (blue). Grey dots correspond to the remaining HVA conductance that was not fully blocked by the cocktail of HVA channel inhibitors. E mean maximal macroscopic conductance values (G$_{max}$) for HVA (black circles) and LVA (blue circles) currents, obtained by fitting the I/V curves with a modified Boltzmann equation (eq. 1). F mean normalized voltage-dependence of activation for HVA and LVA currents. G mean half-activation potential values obtained from the activation curve fits using a modified Boltzmann equation (eq. 2). H Representative time course of HVA calcium current amplitude in response to sequential application of various HVA channel blockers. The inset shows representative HVA calcium current traces in response to the various blockers. I mean maximal inhibition of HVA calcium currents by each blocker.

TTX-insensitive voltage-activated sodium channels. This finding is consistent with previous studies that have reported the presence of Na$_v$1.3 and Na$_v$1.6 channels in human spinal motor neurons [18,19]. Additionally, we confirmed the functional expression of voltage-activated potassium channels (Figure 6 (d,e)). While we did not identify the exact molecular composition of these channels, our findings align with previous studies in human spinal motor neurons, which reported mRNA expression of *KCNQ2*, *KCNA1*, and *KCNA2*, encoding K$_v$7.2, K$_v$1.1, and K$_v$1.2 channels, respectively [20].

Discussion

Human induced pluripotent stem cell (iPSC)-derived motor neurons represent a valuable tool for investigating disease mechanisms and developing potential novel therapeutics. In this study, we characterized the electrophysiological properties of commercially available iPSC-derived motor neurons to evaluate their maturation and functional relevance. Our findings highlight their potential while also identifying areas for further optimization.

The iPSC-derived motor neurons expressed key protein biomarkers such as MNX1/HB9, Tuj1, CHAT, and MAP2 which are essential for confirming their identity as motor neurons [21]. Moreover, these markers indicate that the cells are on a development trajectory consistent with mature motor neurons. However, additional analysis of the expression of other motor neuron specific markers such as SMI-32 [22], combined with more advanced morphological assessments [23] could provide a more comprehensive picture of their level of maturity.
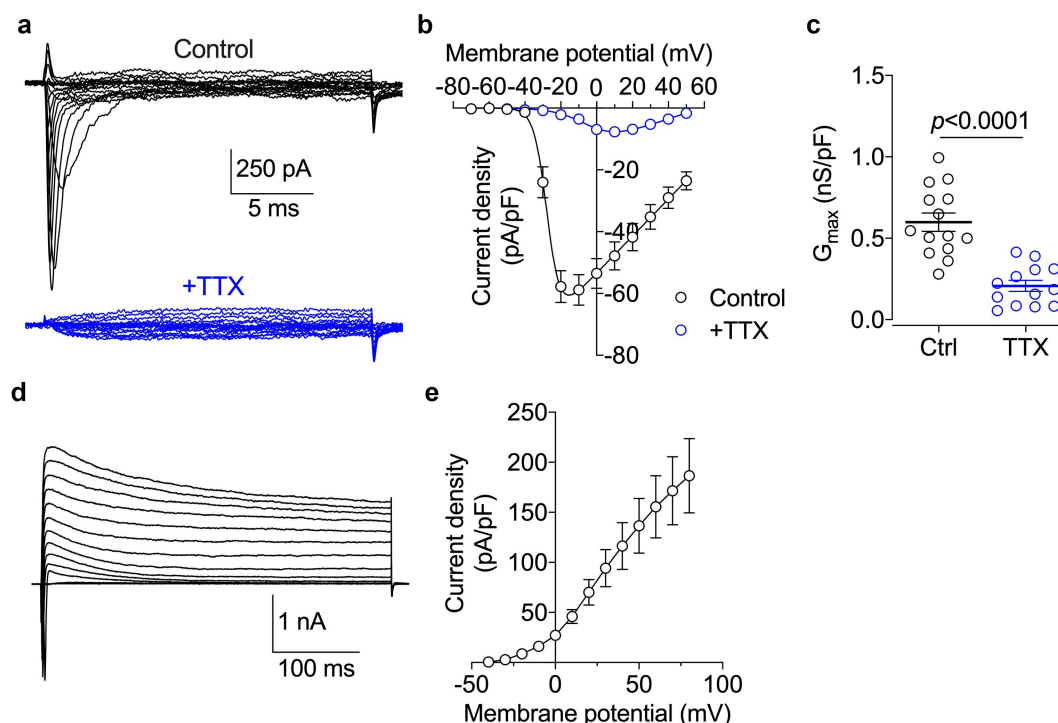
Figure 6. Voltage-activated sodium and potassium current analysis of iPSC-derived motor neurons. A Representative voltage-activated sodium current traces recorded from iPSC-derived motor neurons at DIV 10. Currents were elicited by 20-ms depolarizing steps ranging from −70 mV to +50 mV, applied from a holding potential of −100 mV. Traces are shown before (black) and after (blue) application of 1 mm TTX. B corresponding mean *I/V* relationships for sodium currents, with and without TTX. C corresponding mean maximal macroscopic conductance values (G_{max}) for Nav currents before (black circles) and after TTX application. D Representative voltage-activated potassium current traces recorded from iPSC-derived motor neurons at DIV 10. Currents were elicited by 400-ms depolarizing steps ranging from −40 mV to +80 mV, applied from a holding membrane potential of −60 mV. E corresponding mean *I/V* relationship for potassium currents.

Electrophysiological recordings revealed some limitations in the passive membrane properties of these neurons. The input resistance of the iPSC-derived motor neurons was significantly higher than that reported for primary motor neurons [24,25]. However, similar findings were reported in mouse neonatal sympathetic preganglionic neurons where the input resistance ranged from 260 MΩ to 2600 mΩ with an average of 1140 MΩ [26]. In this study, a high input resistance was associated with lower repetitive firing frequencies which appears to be consistent with our findings on motor neurons where repetitive firing was not pronounced. This observation suggests that these neurons may not have fully matured electrically, as the input resistance typically decreases during development. Additionally, the resting membrane potential (RMP) was more depolarized than expected for mature motor neurons [27], which could further indicate a degree of immaturity.

While an increase in firing rates from DIV 5–8 to DIV 9–15 suggests continued maturation, the cultures showed signs of deterioration after DIV 12. For instance, we observed an increase in dying cells, a reduced number of neurites, and signs of plasma membrane damage. Electrophysiologically, the cells were challenging to seal, exhibited increased leak current, and showed unstable recordings. This observation aligns with the manufacturer's recommendation to use these neurons only up to DIV 10. Extending the culture period to achieve greater maturation, as seen in other studies using iPSC-derived motor neurons, was not feasible under the provided conditions. This limitation highlights the need to refine the current protocols and media to support longer-term cultures as achieved in previous studies [28–30]. Nonetheless, the firing patterns observed in our study were consistent with those reported for other iPSC-derived motor neuron models, including those cultured in motor

neuron-specific or co-culture media [29–31]. This similarity suggests that the electrophysiological properties of these commercially available neurons are comparable to more established systems, offering a convenient alternative for research. We note that our study was conducted across three batches of iPSCs, with no noticeable differences between them. This consistency is expected, as all three batches originated from the same initial preparation and were cultured under identical conditions. However, the limited availability of data on the electrophysiological properties of other commercially available iPSC-derived motor neurons makes direct comparisons challenging. Of the few studies that have assessed such neurons, detailed patch-clamp data remain sparse, underscoring the need for further characterization.

The presence of high-voltage-activated calcium currents including L-type, N-type, P/Q-type and R-type channels was confirmed and consistent with previous studies [32]. Moreover, we observed the presence of small low-voltage-activated T-type currents. While these currents were comparatively very small compared to HVA calcium currents, it is interesting to note that previous studies have suggested their implication in the development of rare cases of ALS [33,34]. Finally, we confirmed the presence of voltage-activated potassium currents, as well as the presence of both TTX-sensitive and TTX-insensitive voltage-gated sodium channels. TTX-sensitive sodium channels are typically associated with fast, transient sodium currents that contribute to the upstroke of action potentials, while TTX-insensitive channels, such as $Na_v1.5$, $Na_v1.8$, or $Na_v1.9$, are less common in motor neurons but may play a role in sustained excitability or specialized signaling functions [16].

While this study provides valuable insights, additional validation is necessary to fully realize the potential of these neurons. Co-culture systems incorporating astrocytes and muscle fibers should be explored to promote full maturation and functional integration [2,28,29,35]. Furthermore, extending the culture period under optimized conditions could enable these neurons to achieve electrophysiological properties more comparable to primary motor neurons or other mature iPSC-derived motor neuron models. Another avenue for future research involves assessing synaptic connectivity and network activity, which are critical for modeling motor neuron function

in vivo. Investigating how these neurons respond to disease-specific conditions or pharmacological interventions could also provide insights into their utility in drug discovery and therapeutic development.

In conclusion, this study highlights the electrophysiological potential of commercially available iPSC-derived motor neurons as a promising platform for modeling motor neuron function and disease states. These neurons exhibit several hallmark features of motor neuron physiology, including the expression of key ion channels and maturation-associated changes in excitability. However, limitations in culture longevity and full maturation underscore the need for protocol refinement and co-culture strategies. With further validation and optimization, these neurons could provide a valuable resource for bypassing traditional differentiation protocols, accelerating drug discovery, and advancing our understanding of motor neuron disorders.

Disclosure statement

Funding

Abbreviations

ALS	Amyotrophic lateral sclerosis
AP	Action potential
CHAT	Choline acetyltransferase
HB9	Homeobox HB9
HVA	High-voltage-activated
iPSC	Induced pluripotent stem cell
LVA	Low-voltage-activated
MAP2	Microtubule-associated protein 2
MND	Motor neuron disease
MNX1	Motor neuron and pancreas homeobox 1
SMA	Spinal muscular atrophy

Authors' contributions

B.J.T. performed the electrophysiology and analyzed the data. Z.S.T. performed the immunostaining and confocal microscopy. R.N.S. contributed to the analysis of electrophysiological data. N.W. wrote the manuscript. All authors critically revised the manuscript and contributed significantly to this work. All authors read and approved the final manuscript.

Data availability statement

All data generated or analyzed in this study are included in this published article. Additional information and materials can be obtained from the corresponding author upon reasonable request.

ORCID

Bohumila Jurkovicova-Tarabova　　http://orcid.org/0000-0002-7931-922X
Robin N. Stringer　http://orcid.org/0000-0002-0887-7670
Zuzana Sevcikova Tomaskova　http://orcid.org/0000-0003-2104-8823
Norbert Weiss　http://orcid.org/0000-0002-0040-1109

References

[1] Li L, Chao J, Shi Y. Modeling neurological diseases using iPSC-derived neural cells: iPSC modeling of neurological diseases. Cell Tissue Res. 2018;371 (1):143–151. doi: 10.1007/s00441-017-2713-x

[2] Johns AE, Maragakis NJ. Exploring motor neuron diseases using iPSC platforms. Stem Cells. 2022;40 (1):2–13. doi: 10.1093/stmcls/sxab006

[3] Tsitkov S, Valentine K, Kozareva V, et al. Disease related changes in atac-seq of iPSC-derived motor neuron lines from ALS patients and controls. Nat Commun. 2024;15(1):3606. doi: 10.1038/s41467-024-47758-8

[4] Egawa N, Kitaoka S, Tsukita K, et al. Drug screening for ALS using patient-specific induced pluripotent stem cells. Sci Transl Med. 2012;4(145):145ra104. doi: 10.1126/scitranslmed.3004052

[5] Little D, Ketteler R, Gissen P, et al. Using stem cell–derived neurons in drug screening for neurological diseases. Neurobiol Aging. 2019;78:130–141. doi: 10.1016/j.neurobiolaging.2019.02.008

[6] Amorós MA, Choi ES, Cofré AR, et al. Motor neuron-derived induced pluripotent stem cells as a drug screening platform for amyotrophic lateral sclerosis. Front Cell Dev Biol. 2022;10:962881. doi: 10.3389/fcell.2022.962881

[7] Ito D, Morimoto S, Takahashi S, et al. Maiden voyage: induced pluripotent stem cell-based drug screening for amyotrophic lateral sclerosis. Brain. 2023;146(1):13–19. doi: 10.1093/brain/awac306

[8] Mateos-Aparicio P, Bello SA, Rodríguez-Moreno A. Challenges in physiological phenotyping of hiPSC-derived neurons: from 2D cultures to 3D brain organoids. Front Cell Dev Biol. 2020;8:797. doi: 10.3389/fcell.2020.00797

[9] Workman MJ, Lim RG, Wu J, et al. Large-scale differentiation of iPSC-derived motor neurons from ALS and control subjects. Neuron. 2023;111(8):1191–1204. e5. doi: 10.1016/j.neuron.2023.01.010

[10] Van Lent J, Prior R, Pérez Siles G, et al. Advances and challenges in modeling inherited peripheral neuropathies using iPSCs. Exp Mol Med. 2024;56 (6):1348–1364. doi: 10.1038/s12276-024-01250-x

[11] Rimington RP, Fleming JW, Capel AJ, et al. Bioengineered model of the human motor unit with physiologically functional neuromuscular junctions. Sci Rep. 2021;11(1):11695. doi: 10.1038/s41598-021-91203-5

[12] Fiskum V, Sandvig A, Sandvig I. Silencing of activity during hypoxia improves functional outcomes in motor neuron networks in vitro. Front Integr Neurosci. 2021;15:792863. doi: 10.3389/fnint.2021.792863

[13] Spijkers XM, Pasteuning-Vuhman S, Dorleijn JC, et al. A directional 3D neurite outgrowth model for studying motor axon biology and disease. Sci Rep. 2021;11 (1):2080. doi: 10.1038/s41598-021-81335-z

[14] Bostock H, Sharief MK, Reid G, et al. Axonal ion channel dysfunction in amyotrophic lateral sclerosis. Brain. 1995;118(1):217–225. doi: 10.1093/brain/118.1.217

[15] LoRusso E, Hickman JJ, Guo X. Ion channel dysfunction and altered motoneuron excitability in ALS. Neurol Disord Epilepsy J. 2019;3(2):124.

[16] Stringer RN, Weiss N. Pathophysiology of ion channels in amyotrophic lateral sclerosis. Mol Brain. 2023;16 (1):82. doi: 10.1186/s13041-023-01070-6

[17] Shimojo D, Onodera K, Doi-Torii Y, et al. Rapid, efficient, and simple motor neuron differentiation from human pluripotent stem cells. Mol Brain. 2015;8 (1):79. doi: 10.1186/s13041-015-0172-4

[18] Kubat Öktem E, Mruk K, Chang J, et al. Mutant SOD1 protein increases Nav1.3 channel excitability. J Biol Phys. 2016;42(3):351–370. doi: 10.1007/s10867-016-9411-x

[19] Jørgensen HS, Jensen DB, Dimintiyanova KP, et al. Increased axon initial segment length results in increased Na^+ currents in spinal motoneurones at symptom onset in the G127X SOD1 mouse model of amyotrophic lateral sclerosis. Neuroscience. 2021;468:247–264. doi: 10.1016/j.neuroscience.2020.11.016

[20] Jiang YM, Yamamoto M, Kobayashi Y, et al. Gene expression profile of spinal motor neurons in sporadic amyotrophic lateral sclerosis. Ann Neurol. 2005;57 (2):236–251. doi: 10.1002/ana.20379

[21] Sepehrimanesh M, Ding B. Generation and optimization of highly pure motor neurons from human

induced pluripotent stem cells via lentiviral delivery of transcription factors. Am J Physiol Cell Physiol. 2020;319(4):C771–80. doi: 10.1152/ajpcell.00279.2020

[22] Sanooghi D, Lotfi A, Bagher Z, et al. Large-scale analysis of MicroRNA expression in motor neuron-like cells derived from human umbilical cord blood mesenchymal stem cells. Sci Rep. 2022;12(1):5894. doi: 10.1038/s41598-022-09368-6

[23] Thomson SR, Nahon JE, Mutsaers CA, et al. Morphological characteristics of motor neurons do not determine their relative susceptibility to degeneration in a mouse model of severe spinal muscular atrophy. PLOS ONE. 2012;7(12):e52605. doi: 10.1371/journal.pone.0052605

[24] Glenn LL, Dement WC. Membrane potential and input resistance in alpha motoneurons of hindlimb extensors during isolated and clustered episodes of phasic events in REM sleep. Brain Res. 1985;339(1):79–86. doi: 10.1016/0006-8993(85)90623-7

[25] Glenn LL, Dement WC. Membrane potential and input resistance of cat spinal motoneurons in wakefulness and sleep. Behav Brain Res. 1981;2(2):231–236. doi: 10.1016/0166-4328(81)90060-7

[26] Zimmerman A, Hochman S. Heterogeneity of membrane properties in sympathetic preganglionic neurons of neonatal mice: evidence of four subpopulations in the intermediolateral nucleus. J Neurophysiol. 2010;103 (1):490–498. doi: 10.1152/jn.00622.2009

[27] Meehan CF, Moldovan M, Marklund SL, et al. Intrinsic properties of lumbar motor neurones in the adult G127insTGGG superoxide dismutase-1 mutant mouse in vivo: evidence for increased persistent inward currents. Acta Physiologica. 2010;200(4):361–376. doi: 10.1111/j.1748-1716.2010.02188.x

[28] Stockmann M, Linta L, Föhr KJ, et al. Developmental and functional nature of human iPSC derived motoneurons. STEM Cell Rev And Rep. 2013;9 (4):475–492. doi: 10.1007/s12015-011-9329-4

[29] Taga A, Dastgheyb R, Habela C, et al. Role of human-induced pluripotent stem cell-derived spinal cord astrocytes in the functional maturation of motor neurons in a multielectrode array system. Stem Cells Transl Med. 2019;8(12):1272–1285. doi: 10.1002/sctm.19-0147

[30] Burley S, Beccano-Kelly DA, Talbot K, et al. Hyperexcitability in young iPSC-derived C9ORF72 mutant motor neurons is associated with increased intracellular calcium release. Sci Rep. 2022;12(1):7378. doi: 10.1038/s41598-022-09751-3

[31] Vahsen BF, Gray E, Candalija A, et al. Human iPSC co-culture model to investigate the interaction between microglia and motor neurons. Sci Rep. 2022;12 (1):12606. doi: 10.1038/s41598-022-16896-8

[32] Chang Q, Martin LJ. Voltage-gated calcium channels are abnormal in cultured spinal motoneurons in the G93A-SOD1 transgenic mouse model of ALS. Neurobiol Dis. 2016;93:78–95. doi: 10.1016/j.nbd.2016.04.009

[33] Rzhepetskyy Y, Lazniewska J, Blesneac I, et al. CACNA1H missense mutations associated with amyotrophic lateral sclerosis alter Cav3.2 T-type calcium channel activity and reticular thalamic neuron firing. Channels (Austin). 2016;10(6):466–477. doi: 10.1080/19336950.2016.1204497

[34] Stringer RN, Jurkovicova-Tarabova B, Huang S, et al. A rare CACNA1H Variant associated with amyotrophic lateral sclerosis causes complete loss of Ca$_v$3.2 T-type channel activity. Mol Brain. 2020;13(1):33. doi: 10.1186/s13041-020-00577-6

[35] Tang Y, Liu ML, Zang T, et al. Direct reprogramming rather than iPSC-based reprogramming maintains aging hallmarks in human motor neurons. Front Mol Neurosci. 2017;10:359. doi: 10.3389/fnmol.2017.00359